C. R. Mecanique 346 (2018) 1199–1215

Contents lists available at ScienceDirect

Comptes Rendus Mecanique

www.sciencedirect.com

Affected depth approach to determine the fatigue strength of materials containing surface defects

Anouar Nasr [a,b,*], Wannes Hassine [a], Chokri Bouraoui [c]

[a] LGM, ENIM, Université de Monastir, avenue Ibn-Eljazzar, Monastir 5019, Tunisia
[b] IPEIM, Université de Monastir, avenue Ibn-Eljazzar, Monastir 5019, Tunisia
[c] LMS, ENISO, Université de Sousse, BP264, Erriadh, Sousse 4023, Tunisia

ARTICLE INFO

Article history:
Received 12 June 2018
Accepted 27 August 2018
Available online 17 October 2018

Keywords:
Reliability
Defect
Affected depth
Fatigue limit
HCF criteria

ABSTRACT

This paper explains a novel methodology to determine the High Cycle Fatigue (HCF) reliability of materials with defects. A defect was represented by a semi-spherical void situated at a specimen surface subjected to periodic loading. Then, the Finite Element (FE) method was carried out to find out the stress distribution near the defects for diverse sizes and diverse loadings. The Crossland stress change is studied and interpolated by a mathematical function depending on fatigue limits, defect radius, and profundity from the defect tip. The HCF strength of defect material is computed by the "stress strength" approach via the Monte Carlo sampling. This approach leads to determine Kitagawa–Takahashi diagrams, for a definite reliability, of materials with defects. The calculated HCF reliabilities agree well with fatigue tests. Obtaining Kitagawa–Takahashi diagrams with reliability level permits the engineer to be engaged in an endurance problem to compute the defective fatigue lives in safe and efficient process. As a final point, we discuss the sensitivity effects of defect size, defect free fatigue limits, affected depth, and load amplitude to envisage the fatigue reliability of materials with defects.

1. Introduction

Fatigue is a major causing damage of structures and mechanical components in several engineering fields, such as aeronautic, automotive, civil, marine, and mechanical engineering. Fatigue lives are governed by diverse factors such initial flaws, structural geometry, loading types, material properties, etc. Fatigue criteria should include major parameters such as gradient stress, material microstructure, and casting defects. However, all these parameters are in essence random and not correctly controllable. Hence, reliability-based approaches are necessary to make sure a predictable safety when fatigue lives are assessed.

Agha and Chantier [1,2] suggested a probabilistic HCF approach for an automotive nodular cast iron. Defects were symbolized by a pre-existent circular micro cracks. Defect sizes distribution is observed experimentally and modeled by a distribution density function. The loading and the number of cycles guide to determine the critical circular crack size. Then, the probability of failure of a representative elementary volume is identified by the probability to enclose defect sizes bigger

* Corresponding author at: LGM, ENIM, Université de Monastir, avenue Ibn-Eljazzar, Monastir 5019, Tunisia.
E-mail address: anouar.nasr@hotmail.fr (A. Nasr).

https://doi.org/10.1016/j.crme.2018.08.012
1631-0721/

Nomenclature

a_w	Affected depth at the fatigue limit	µm
$\sqrt{area}$	Equivalent defect size of defect perpendicular to the direction of the maximum principal stress	µm
C_v	Variation coefficient	
f	Yield surface function	
HCF	High Cycle Fatigue	
HLP	Highest Loaded Plane	
N	Full number of simulation events	
P_f	Failure probability	
R	Defect radius	
r	Length from the defect center into the inside specimen	
$\sqrt{J_{2,a}}$	square root of the second invariant of the stress deviator	MPa
P_{max}	Hydrostatic stress	MPa
R_σ	Load ratio: $R_\sigma = \frac{\sigma_{min}}{\sigma_{max}}$	
$\underline{\underline{S}}(t_i)$ and $\underline{\underline{S}}(t_j)$	Periodic deviator stress tensor in two diverse instants (t_i and t_j)	
α_{Cr}	Coefficient in Crossland criterion	
β_{Cr}	Material parameter in Crossland criterion	MPa
σ_a	Amplitude of the tension loading	MPa
σ_{D-1}	Fatigue limit under fully reversed tension of the defect free material	MPa
σ_{eq}^{Cr}	Crossland equivalent stress	MPa
σ_{max}	Maximum stress of a tension loading	MPa
$\sigma_{D0.1}$	Tension defect-free material fatigue limit under 0.1 load ratio	MPa
τ_a	Amplitude of the torsion loading	MPa
τ_{D-1}	Fatigue limit under fully reversed torsion of the defect free material	MPa

than the critical value. In the end, application of the weakest link theory guide to obtain the reliability of the part [1]. This probabilistic approach is validated only for the studied material and difficult to be extended to other materials because of the big number of employed parameters. Nasr et al. [3] proposed an approach to compute the HCF reliability of an automotive nodular cast iron containing casting defects. FE simulations were carried out for diverse sizes and loadings to illustrate the 3D elastic–plastic stress distribution near the defect. The response surface technique was employed to correlate the hydrostatic stress with the shear stress as a function of the loading amplitude and the defect sizes. The reliability was computed by the stress–strength method via Monte Carlo sampling. Authors have shown that the scattering observed in fatigue tests is caused by the defect distribution. Liu et al. used three reliability-based methods to circumscribe the problems of fatigue crack propagation [4]. The methods are: (i) a First-Order Reliability method (FORM) founded on the Total Derivative Method (TDM), (ii) a FORM founded on the Lagrange Multiplier Formulation (LMF), and (iii) a Monte Carlo sampling with pseudo-exact sampling technique. The crack was followed by a random path that is resolved by a crack direction law. The method of boundary integral element was then used to calculate the mechanical response. The pseudo-exact selection technique was used in MCS to find out an extremely high-accuracy law of probability of failure. Additionally, the transition probability density expression for crack tips was obtained by Oh [5] by solving a diffusion equation, in which diffusion and drift coefficients depended on the laws of crack propagation. The response surface was joined by Leonel et al. [6], using the boundary element method, to evaluate fatigue life. The coupled procedure lets us consider uncertainties during the crack growth process. Additionally, it computes the fatigue failure probability of complex structural geometry and loading. Two coupling processes were considered: (i) direct combination of mechanical solvers and reliability, (ii) indirect combination by the technique of response surface. Liao et al. [7] proposed an approach of dynamic stress–strength interference allowing the non-linear accumulation of fatigue damage. The model was proposed after studying in depth the statistical characteristics of cumulative fatigue damage and its critical value. Because the non-linearity of fatigue damage accumulation has been considered, the model is capable to compute the fatigue strength for arbitrary spectrum loading. To confirm the calculated results, two fatigue experiments were carried out, in which the specimen numbers were up to 100, using fighter spectrum loading (FALSTAFF spectrum) and constant-amplitude loading, respectively. It is demonstrated that the proposed model is consistent and practicable. Xiang et al. [8] proposed a methodology that predicts the general probabilistic life with efficient and accurate fatigue prognosis. The proposed methodology predicts fatigue lives at a given reliability level. It is founded on an inverse first-order reliability method (IFORM). The formulation is different from the forward reliability problem, which aims to estimate the failure probability at a given time instant. The variables in the fatigue prognosis problem were classified into two categories, i.e. random variables and index variables. Calculation of fatigue lives using inverse FORM has been conducted and compared with the direct Monte Carlo results. The methodology proposed was demonstrated and validated by an extensive experimental database. It was shown that the model-predicted results agree well with experimental observations.

Table 1
Mechanical properties and endurance limits of C35 steel and AS7G06-T6 [9,11].

	C35 steel	AS7G06-T6
Young's modulus E	212 GPa	73 GPa
Poisson's ratio ν	0.3	0.3
Monotonic yield strength $R_{p0.2}$	359 MPa	275 MPa
Cyclic yield strength $R_{p0.02cy}$	250 MPa	***
Tensile strength R_m	594 MPa	335 MPa
Tension defect free fatigue limit ($R=-1$) σ_{D-1}	236 MPa	91 MPa
Torsion defect free fatigue limit ($R=-1$) τ_{D-1}	169 MPa	80 MPa

A probabilistic approach that predicts the HCF strength of the defect material is presented in this paper. The model is founded on the influenced length (affected depth) approach. 3D elastic/plastic FE calculations are carried out for diverse defect sizes and different loadings. It leads us to obtain the mathematical expression of the Crossland stress near the defect. Combination of the critical depth approach and of the stress–strength method via the Monte Carlo sampling gives us the HCF strength of the defect material. Probabilistic Kitagawa–Takahashi diagrams are obtained by application of the approach for diverse defect sizes. In the last part of this paper, we present the sensitivity effects of defect size, defect free fatigue limits, affected depth and load amplitude for envisaging the HCF strength of materials with defects.

2. Materials

The proposed approach is validated by using fatigue data of two materials: (i) the cast aluminum alloy AS7G06-T6 and (ii) the C35 steel. The steel experimental tests are obtained from the researches of Nasr and Billaudeau [9,10], while the aluminum alloy experimental tests are tackled from Mu researches [11]. Table 1 shows the fatigue limits and mechanical characteristics of both materials. All the specimens were polished up to grade 4000 paper in order to remove machining marks. The electric Discharge Machining (EDM) process is exploited to machine artificial defects in the center length of a steel fatigue sample [9,10] (Fig. 1a). It permits to control the introduced defects (shape and size). The defective C35 steel fatigue samples are tempered to relax residual stresses occurring during preparation. However, the aluminum alloy AS7G06-T6 contains natural casting defects that are principally shrinkages (Fig. 1b) and artificial defects. The analyses of the specimens, after fatigue tests, through fractographic Scanning Electron Microscope (SEM) observations reveal the type and the size of the defect that leads to failure. Aluminum alloy specimens have undergone thermal treatment in the T6 condition [11]. It consists of: solution heat treatment at 540°C for 10 h, quenching in cold water, aging at room temperature for 24 h, and then aging at 160°C for 8 h.

For defect-free materials, the S–N curves are fitted with the least square method and plotted by using the Stromeyer model [10]. Also defect free fatigue limits at 10^7 cycles (σ_{D-1} and τ_{D-1}) are determined by the staircase method [10]. The step method is applied to find out the endurance limits of the tested materials with defects [9,10]: one specimen will be used to determine the fatigue limit for each defect size for an infinite number of cycles. We load the specimen up to 10^7 cycles; if failure does not occur, the following loading is 10 MPa or 20 MPa higher (one step). This method is obviously not the most accurate one to determine a fatigue limit because of the coaxing effect. A comparison between the standard estimation of the fatigue limit with the staircase method and the step method gives similar values for the C35 steel. The Murakami parameter "$\sqrt{area}$" is exploited to illustrate the defect size [12] where the size is characterized by the root square of the 'area' parameter ('area' of the defect projected on the plane perpendicular to the direction of the maximum principal stress).

3. Crossland criterion

A number of criteria are suggested to evaluate fatigue life materials without defects. The Crossland criterion [13] is employed in this work. It is successfully tested for many materials. It is characterized by an equivalent stress, σ_{eq}^{Cr}, announced as follows:

$$\sigma_{eq}^{Cr} = \sqrt{J_{2,a}} + \alpha_c \, P_{max} \leq \beta_c \tag{1}$$

$\sqrt{J_{2,a}}$ is the square root of the second invariant of the stress deviator. It is obtained as follows:

$$\sqrt{J_{2,a}} = \frac{1}{2\sqrt{2}} \max_{t_i \in T} \left\{ \max_{t_j \in T} \sqrt{\left(\underline{\underline{S}}(t_i) - \underline{\underline{S}}(t_j)\right) : \left(\underline{\underline{S}}(t_i) - \underline{\underline{S}}(t_j)\right)} \right\} \tag{2}$$

where $\underline{\underline{S}}(t_i)$ and $\underline{\underline{S}}(t_j)$ are the periodic deviator stress tensors in two diverse instants (t_i and t_j).

P_{max} is the hydrostatic stress. It is obtained as follows:

$$P_{max} = \frac{1}{3} \max_{t \in T} \left\{ \sigma_{11}(t) + \sigma_{22}(t) + \sigma_{33}(t) \right\} \tag{3}$$

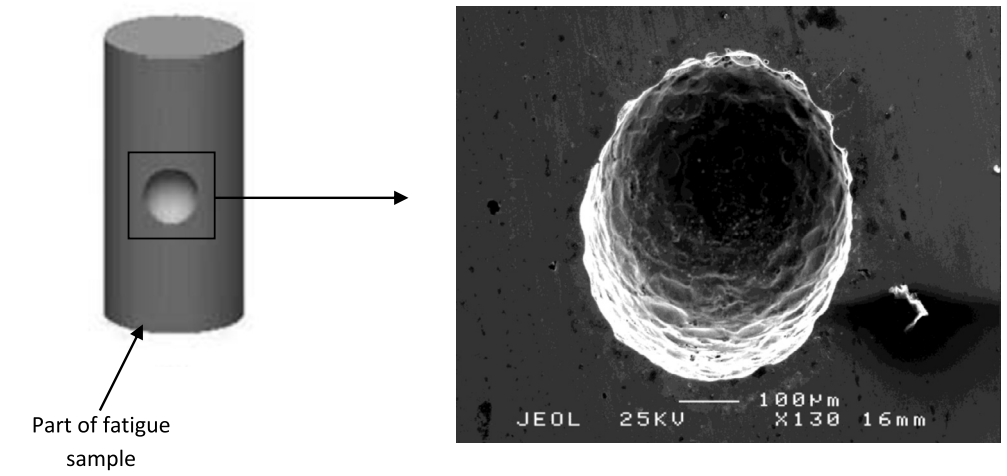

(a)

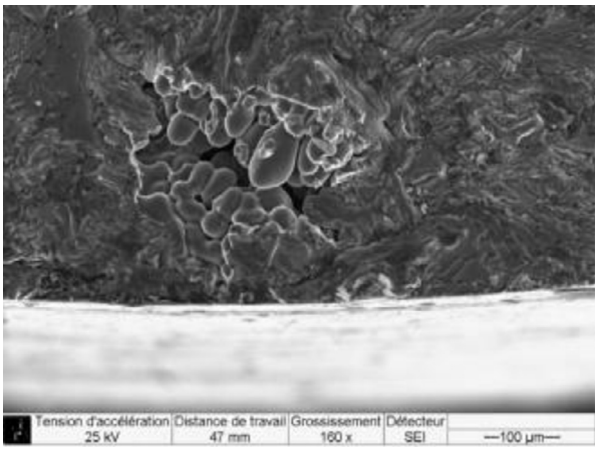

(b)

Fig. 1. (a) Geometry and position of artificial defects on the steel fatigue sample [10]; (b) AS7G06-T6 aluminum alloy presenting natural surface shrinkage [11].

α_c and β_c are two parameters calculated from fatigue limits (σ_{D-1}, τ_{D-1}).

$$\alpha_c = \frac{\tau_{D-1} - \frac{\sigma_{D-1}}{\sqrt{3}}}{\frac{\sigma_{D-1}}{3}} \tag{4}$$

$$\beta_c = \tau_{D-1} \tag{5}$$

4. Stress calculation near the defect

4.1. Finite element modeling

Stress applied to a specimen that contains a defect gives rise to additional stress over and above the nominal applied stress. Indeed, fatigue cracks, which lead to failure, always initiate from these singularities. Hence, it is required to determine the stress field near the defect. Exploiting the FE technique ensures this task. Considering loading and geometry symmetries, the completed model is simplified. Fig. 2 shows loads and boundary conditions of simplified parts under torsion and tension loadings. The four nodes linear tetrahedral solid elements C3D4 are employed to mesh the simplified parts. Meshing is refined and optimized around the defects (Fig. 3a). Cyclic FE calculations are carried out using an elastic/plastic model. The material cyclic stabilized strain–stress curve is used (Fig. 3b and c). The material behavior is modeled by a combined cyclic hardening behavior law. It combines non-linear kinematics and the isotropic hardening laws. Comparison of the stress state given by the simplified and the complete models show a difference lower than 4%.

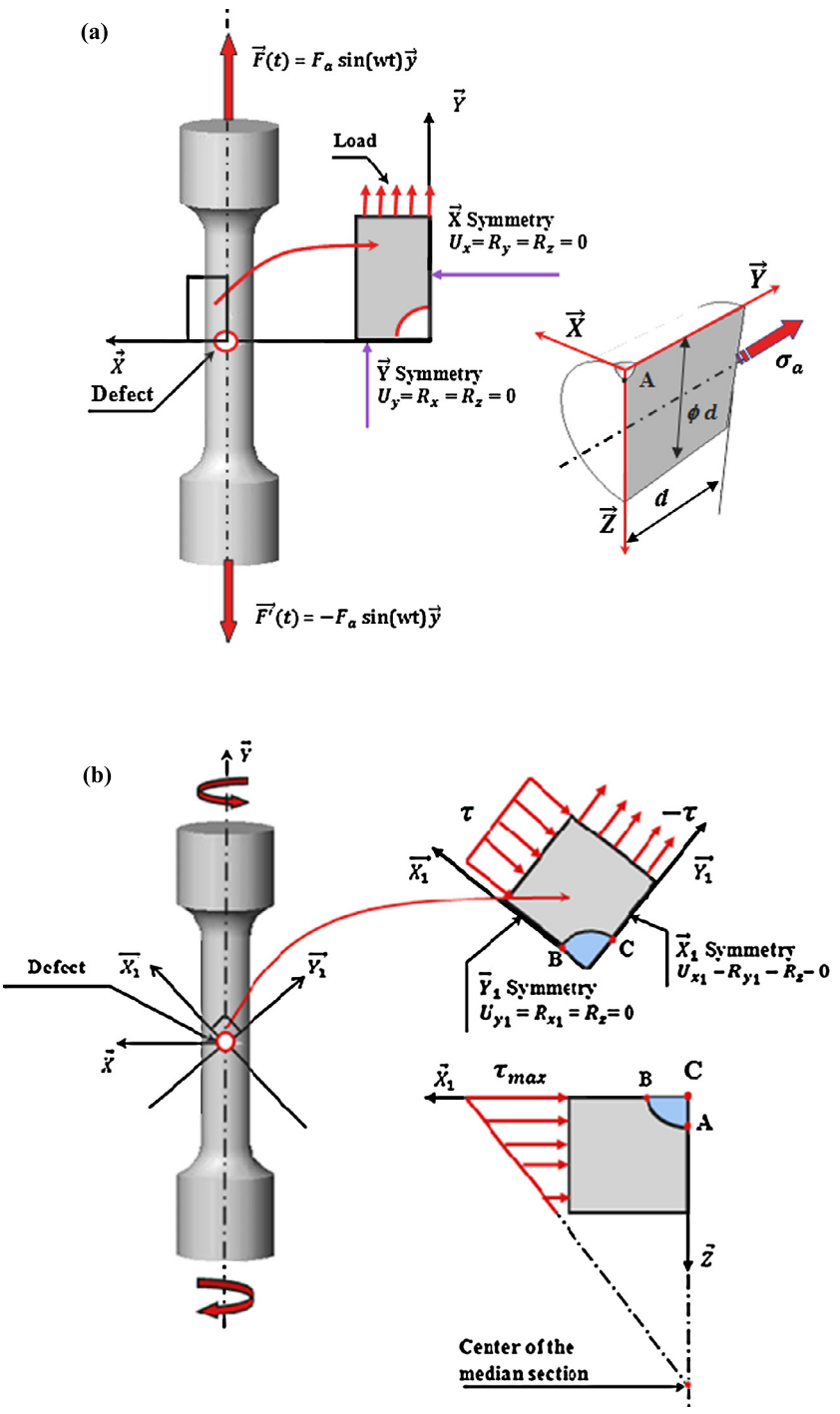

Fig. 2. Completed and simplified model with load and boundary conditions: (a) tension loading; (b) torsion loading.

4.2. Analysis of FE calculation

The purpose of this part is to find out and explore the stress distribution near the defect. Analysis of FE results explain that the state of the stress is multiaxial in front of the defect, even though the loading applied is uniaxial. With the purpose of considering the defect stress multiaxiality, the Crossland stress (σ_{eq}^{Cr}) is used. FE results explain that the plane perpendicular to the maximum principal stress direction is the Highest Loaded Plane (HLP) (Fig. 4). Such remark is also proved by Billaudeau el al. [14]. They show that, for a material with defects subjected to fatigue loading, the crack initiates

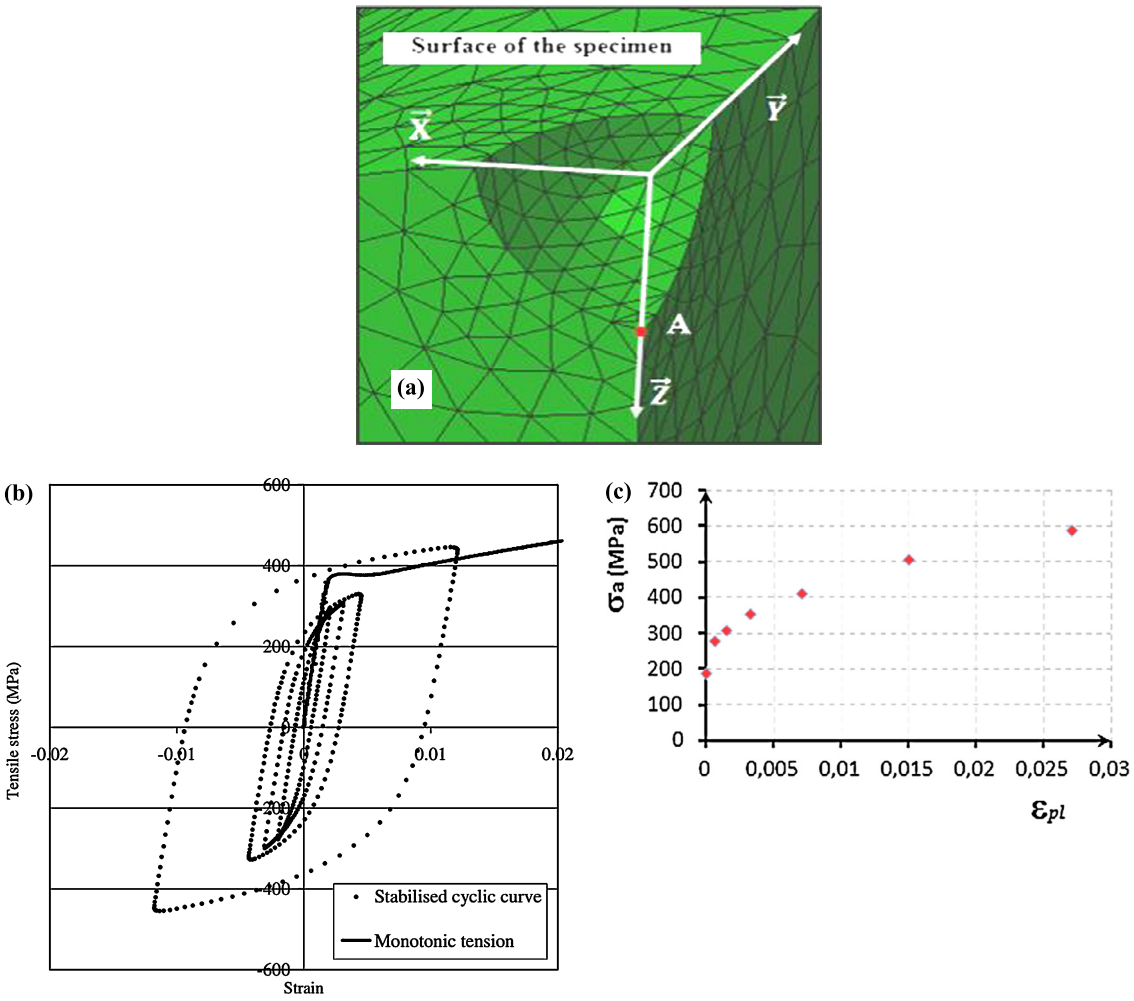

Fig. 3. (a) Refined mesh in front of a defect, (b) monotonic and cyclic tension curves, (c) plastic stress–strain cyclic stabilized curve (experimental result for the C35 material without defect) [14].

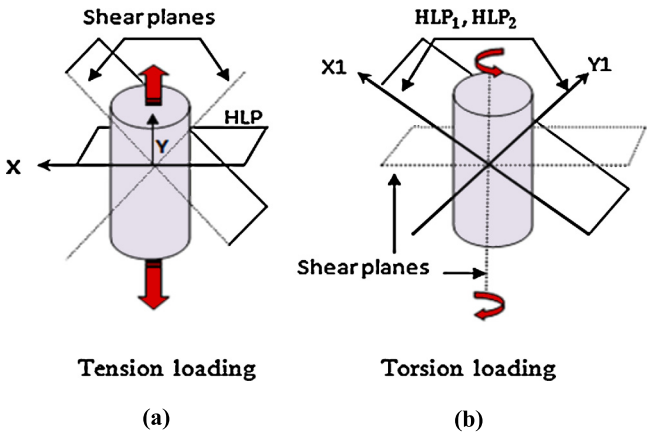

Fig. 4. Shear and highest load planes: (a) tension loading, (b) torsion loading.

at the defect's tip and propagates perpendicularly to the direction of the maximum principal stress (Fig. 5a). For that reason, we chose to study the Crossland stress variation in the HLP from the defect tip into the inside specimen (Fig. 5b). The Crossland stress amplitude in the HLP is determined for fully reserved tension and torsion loadings. The Crossland stress

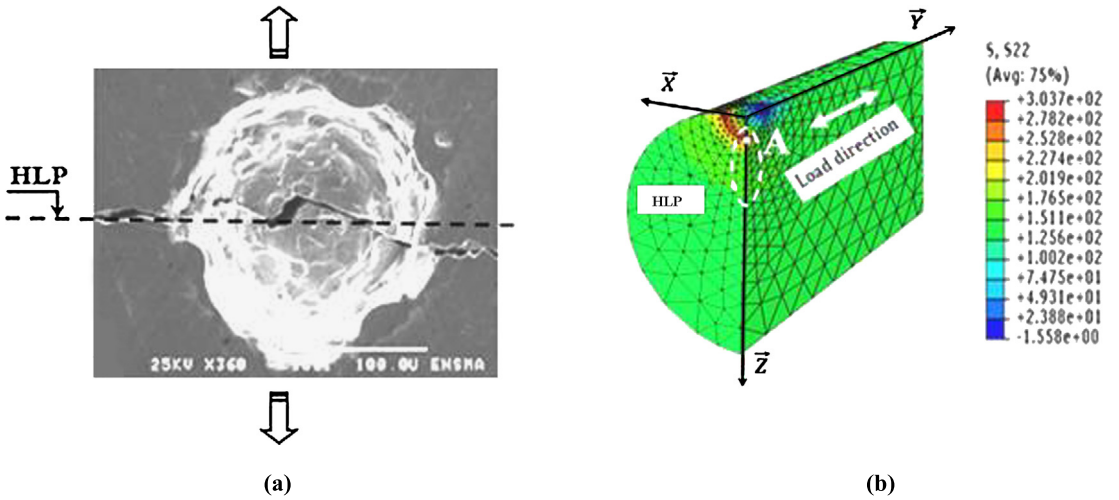

Fig. 5. (a) Crack initiation at the defect tip (tension loading) [14], (b) stress distribution in front of a defect (tension loading).

amplitude (σ_{eq}^{Cr}) can be interpolated, by mathematical expressions including the applied load amplitude, ($\frac{\tau_{D-1}}{\sigma_{D-1}}$) and ($r/R$) ratios, where R is the defect's radius and r is the length from the defect's center to the inside specimen. For an alternate tension load, σ_{eq}^{Cr} can be modeled (interpolated) by the following relationship:

$$\sigma_{eq}^{Cr}(r) = \frac{\tau_{D-1}}{\sigma_{D-1}} * \sigma_a \times \left(\frac{1}{(r/R)^4} + 1 \right) \tag{6}$$

For alternate torsion load, σ_{eq}^{Cr} can be modeled by:

$$\sigma_{eq}^{Cr}(r) = \frac{\tau_{D-1}}{\sigma_{D-1}} * \tau_a \times \left(\frac{1}{(r/R)^2} + 1 \right) \tag{7}$$

Equations (6) and (7) group mechanical and geometrical parameters of the study, worth knowing the material fatigue limits (σ_{D-1}, τ_{D-1}), the load amplitude (σ_a or τ_a), the defect radius (R) and the depth r.

5. Affected depth approach

FE computations have been conducted by Nasr et al. for materials with defects subjected to periodic loadings [15]. The authors studied, on the high loaded plane, the Crossland stress change in front of the defect for many specimens including a surface defect and submitted to their experimental defective fatigue limit. Fig. 6 explains the change of Crossland stress, from the defect tip to the inside sample, for three sizes. Each specimen is subjected to its experimental defective fatigue limit. Fatigue limits are 135 MPa for $\sqrt{area} = 900$ µm, 150 MPa for $\sqrt{area} = 400$ µm and 195 MPa for $\sqrt{area} = 170$ µm (experimentally identified). Three curves show a common intersection point (point H) at ≈ 50 µm length from the defect's tip [15]. At the common intersection point, the Crossland stresses have the same value of β_c (τ_{D-1}). The authors conclude that, under an endurance limit load, the stress of Crossland at the point H (intersection point) is independent of $\sqrt{area}$. Also, for an endurance limit load, the affected depth (a_w) appears to be stable in spite of $\sqrt{area}$. Consequently, the length from the defect tip to the common intersection point can be regarded as a critical length (depth) that used to compute endurance limits of materials with defects [15]. Nasr et al. [15] show that the defective fatigue limit may be estimated by the Crossland stress at a profundity a_w from the defect. For a specified defect under a certain load, if the Crossland stress at a_w depth is less than β_c, there is no failure. Otherwise, the part will be broken before 10^7 cycles. The fatigue limit of a sample containing a surface defect corresponds to:

$$\sigma_{eq}^{Cr}(a_w) = \beta_c \tag{8}$$

where: σ_{eq}^{Cr} is the equivalent stress of Crossland, a_w is a critical length. It is a material parameter made out from an experimental endurance limit of the defect material [15].

The proposed approach has been applied to the C35 and the AS7G03-T6 materials containing spherical and elliptical defects and submitted to various loadings. The computed results illustrate excellent agreement with experimental tests [15]. The benefit of the approach consists in being multiaxial and it can be applied for diverse load ratios. However, it is a deterministic approach. Consequently, it is important to incorporate the input parameters' scattering effect.

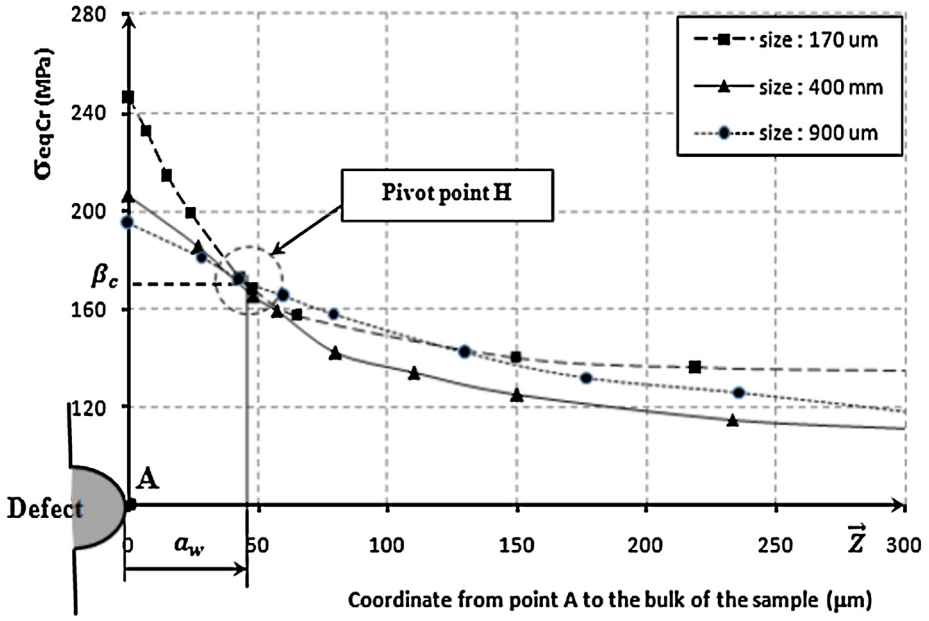

Fig. 6. Variation of Crossland stress along the $\vec{Z}$-axis for three defect sizes under tension endurance limits (C35 steel, spherical pore) [15].

6. HCF strength computation

6.1. Methodology

6.1.1. Monte Carlo sampling

To compute the reliability, a vector of arbitrary variables $\{X\}$ is considered to represent uncertain structural numbers or quantities. x_i is an element of the arbitrary vector $\{X\}$. $f_{X_i}(x_i)$ is its probability density function (PDF). $G(\{x\})$ is a performance function that separates security and failure fields; it is written as follows:

$$G(\{x\}) = S(\{x\}) - L(\{x\}) \tag{9}$$

$G(\{x\}) = 0$ represents the limit state function, $S(\{x\})$ is the strength function, and $L(\{x\})$ is the load function [16,17]. The probability of failure P_f is given by:

$$P_f = \int_{G(\{x\})<0} f_{\{X\}}(\{x\})\mathrm{d}x_1 \ldots \mathrm{d}x_n = \Pr\big(L(\{x\}) > S(\{x\})\big) = \Pr\big(G(\{x\}) < 0\big) \tag{10}$$

Using several random selections, the Monte Carlo method aims to simulate a high number of load and strength values according to their PDF. N is the full number of simulation events. For the N calculated values of $G(\{x\})$, it is assumed that the failure event frequency, where $G(\{x\}) < 0$, extends towards the failure probability P_f when $N \to +\infty$ [17].

$$P_f = \lim_{N\to+\infty} \frac{\text{Number of failure events } (G(\{x\}) < 0)}{N} \tag{11}$$

For a definite coefficient of variation of P_f equal to 0.1 and for $P_f = 10^{-n_0}$, the Monte Carlo sampling number needed is $N = 10^{n_0+2}$ (i.e. $P_f = 0.01$, $N = 10{,}000$) [16,18].

In this article, N is taken equal to 10,000, it is an acceptable computational cost, especially for analytic function. It is noted that the random sampling number is chosen after studying the convergence of the reliability in stable results. The proposed approach permits to consider the scattering of several parameters (material parameters and load variation) on the HCF strength. The reliability is given by the next relationship:

$$\textit{Reliability} = \lim_{N\to+\infty} \frac{\text{Number of safety events } (G(\{x\}) > 0)}{N} = 1 - P_f \tag{12}$$

6.1.2. HCF strength computation

The HCF strength of a material containing surface defects will be calculated by the "strength load" approach via Monte Carlo sampling. The load function is the stress of Crossland in the critical depth a_w. The strength function is β_c (τ_{D-1})

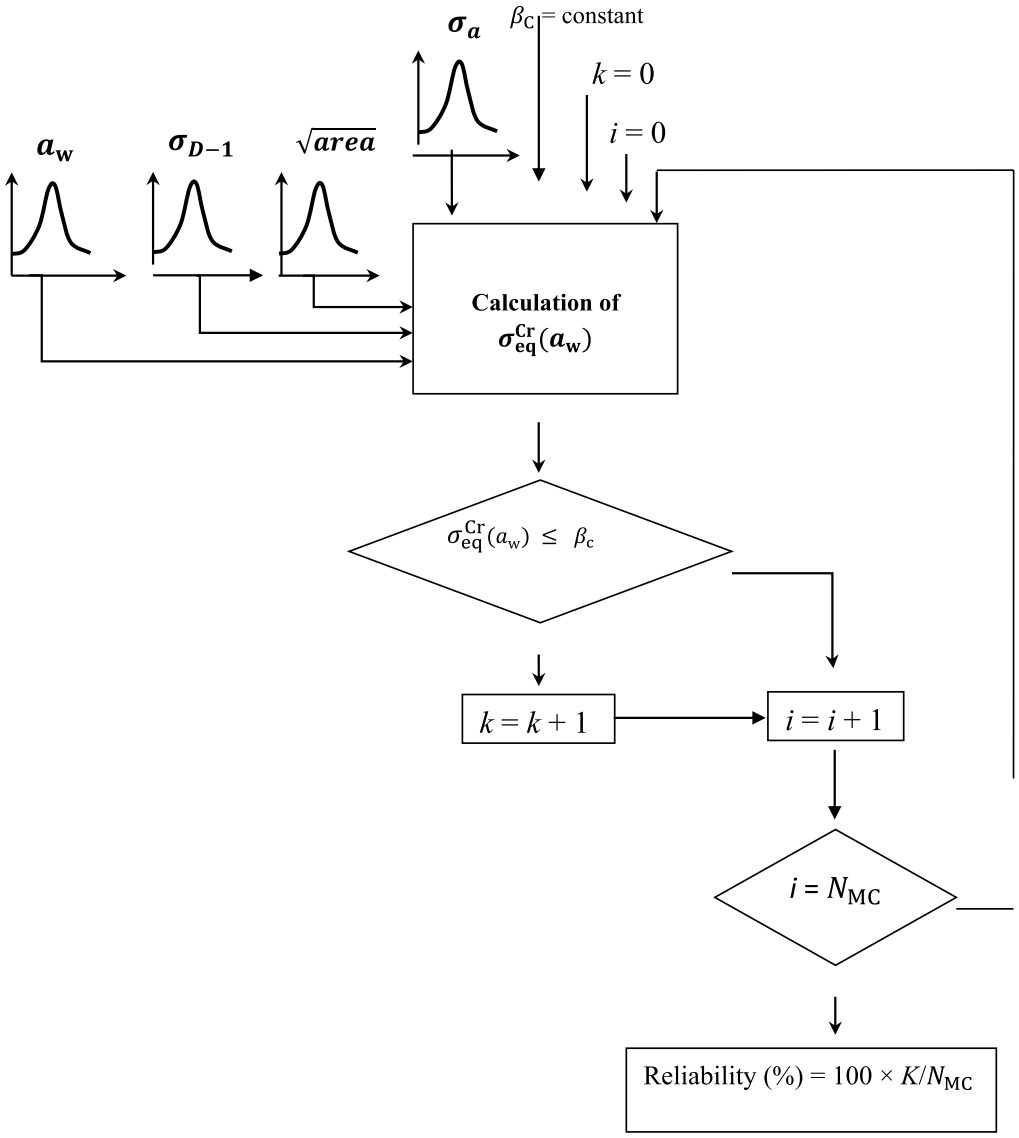

Fig. 7. Organization chart of the calculation of the reliability using the Monte Carlo method.

(Eq. (8)). The scattered input parameters are: a_w, σ_{D-1}, σ_a, and $\sqrt{area}$. The fatigue limit scatters are modeled by normal distributions with 5% of coefficient of variation. The choice of a Gaussian function for fatigue limits is justified by many authors, such as [19–22]. Also, a statistical analysis of defect-free fatigue limits gives a coefficient of variation close to 5%. The identification of the density functions and of the coefficient of variation of the other input parameters requires many tests that cannot be conducted systematically because they are very long and tedious. To simplify this task, all input parameters are assumed to take a normal distribution with a coefficient of variation of 5%. It is noted that the proposed approach allows choosing another density function with any coefficient of variation.

A great number of random selections of input parameters (10,000) selected in view of their probability density functions are realized. For each random selection, the Crossland stress in the critical depth will be calculated using its interpolating equation (Eq. (6) or (7)). The HCF strength is the case number where the Crossland stress is lower than β_c divided by random sampling numbers. Fig. 7 shows the organization chart adopted to calculate the HCF strength of a material with defects. The same calculation is repeated for several levels of load. It leads to obtaining the change of the reliability versus the load amplitude for a definite defect. Figs. 8 and 9 represent the obtained results, respectively, for the steel containing 400-μm defect size and for the aluminum alloy containing 700-μm defect size.

According to Crossland criterion, $\beta_c = \tau_{D-1}$. This parameter exists on both sides in the interpolated equation (Eq. (8)). Thus, it is simplified, and its scatter is ineffective on the calculation of the reliability. Consequently, the parameter τ_{D-1} is a relevant parameter for fatigue lifetime prediction, but its scatter does not influence HCF reliability.

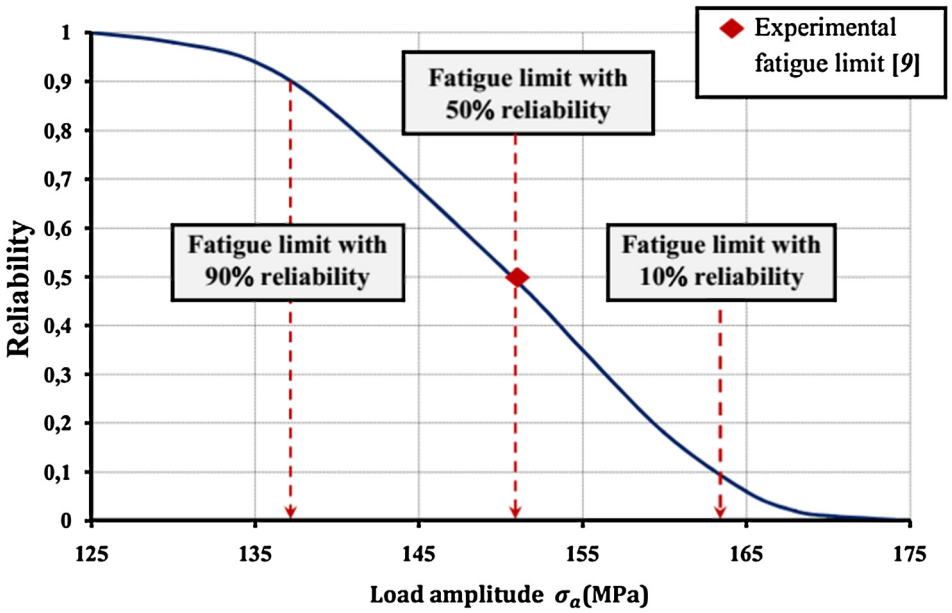

Fig. 8. HCF reliability prediction of the C35 steel under loading ($R_\sigma = -1$, $\sqrt{area} = 400$ µm).

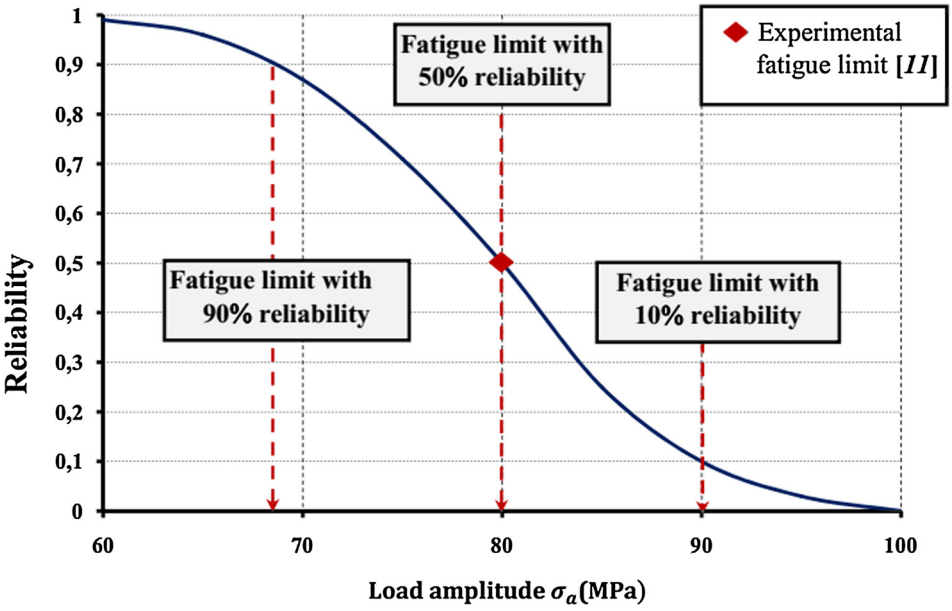

Fig. 9. HCF reliability prediction for the AS7G03-T6 alloy under tension loading ($R_\sigma = -1$, $\sqrt{area} = 700$ µm).

6.2. Applications

6.2.1. Tension loading ($R_\sigma = -1$)

For tension load, the variation of the Crossland stress, from the defect's tip to the specimen's bulk, is interpolated by:

$$\sigma_{eq}^{Cr}(r) = \frac{\tau_{D-1}}{\sigma_{D-1}} \times \sigma_a \times \left(\frac{1}{(r/R)^4} + 1 \right) \tag{13}$$

where R is the defect's radius and r is profundity from the defect's center. In the critical depth, r is equivalent to the defect radius plus the critical defect depth ($r = R + a_w$). Therefore, the equation below becomes:

$$\sigma_{eq}^{Cr}(a_w) = \frac{\tau_{D-1}}{\sigma_{D-1}} \times \sigma_a \times \left(\frac{1}{(R + a_w/R)^4} + 1 \right) \tag{14}$$

Table 2
Critical depth, fully reversed tension fatigue limit and their low distributions for the C35 and AS7G06-T6 materials.

Material	Parameter	Distribution	Mean	C_v
C35	a_w (μm)	Normal	50	5%
	σ_{D-1} (MPa)	Normal	236	5%
AS7G06-T6	a_w (μm)	Normal	360	5%
	σ_{D-1} (MPa)	Normal	91	5%

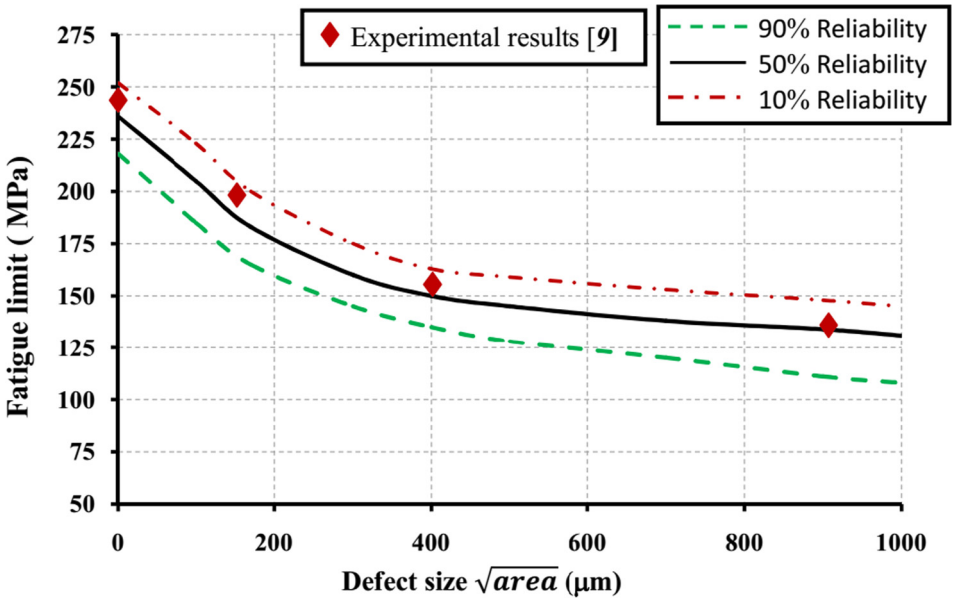

Fig. 10. Probabilistic Kitagawa–Takahashi diagram under tension fatigue loading for the steel.

Table 3
Critical depth, fatigue limit under 0.1 load ration and their low distributions for the C35 and AS7G06-T6 materials.

Material	Parameter	Distribution	Mean	C_v
C35	a_w (μm)	Normal	70	5%
	$\sigma_{D0.1}$ (MPa)	Normal	410	5%
AS7G06-T6	a_w (μm)	Normal	160	5%
	$\sigma_{D0.1}$ (MPa)	Normal	145	5%

Table 2 defines the critical depth, the fully reversed fatigue limits and their low distributions for the C35 and AS7G06-T6 materials. The input parameters (a_w, σ_{D-1}, σ_a, and $\sqrt{area}$) are assumed to take normal distribution with a coefficient of variation (C_v) of 5%. The reliability curves are calculated for diverse defect sizes. This leads to obtain a probabilistic change of endurance limit versus defect size. Kitagawa–Takahashi diagrams are calculated for reliabilities of 10, 50, and 90% under tension and torsion loadings. The computed results are represented in Figs. 10 and 11, respectively, for the C35 and the AS7G03-T6 materials.

6.2.2. Repeated tension ($R_\sigma = 0.1$)

For alternate tension load, σ_{eq}^{Cr} can be interpolated by:

$$\sigma_{eq}^{Cr}(r) = \frac{\tau_{D-1}}{\sigma_{D0.1}} \times \sigma_{max} \times \left(\frac{1}{((r)/R)^4} + 1 \right) \tag{15}$$

At a depth a_w, the equation below becomes:

$$\sigma_{eq}^{Cr}(a_w) = \frac{\tau_{D-1}}{\sigma_{D0.1}} \times \sigma_{max} \times \left(\frac{1}{((R + a_w)/R)^4} + 1 \right) \tag{16}$$

Compared to Eq. (14), Eq. (16) shows that σ_a and σ_{D-1} are replaced respectively by σ_{max} and $\sigma_{D0.1}$.

Steel and aluminum input parameters (a_w, $\sigma_{D0.1}$, σ_{max}, and $\sqrt{area}$) are represented by normal distributions having a $C_v = 5\%$ (Table 3). Figs. 12 and 13 show the calculated results.

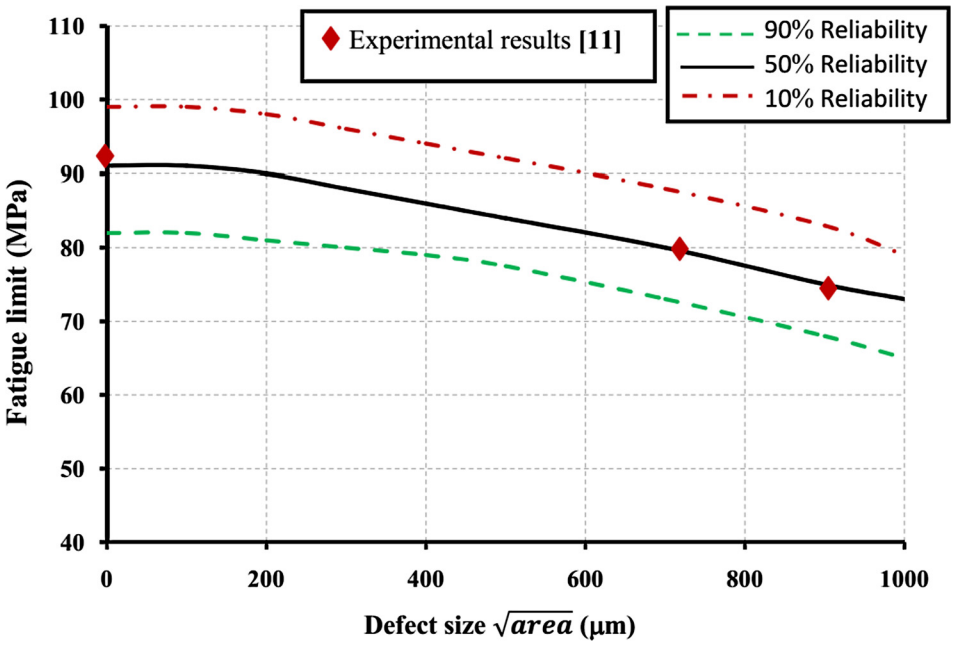

Fig. 11. Probabilistic Kitagawa–Takahashi diagram under tension loading for the AS7G06-T6 alloy.

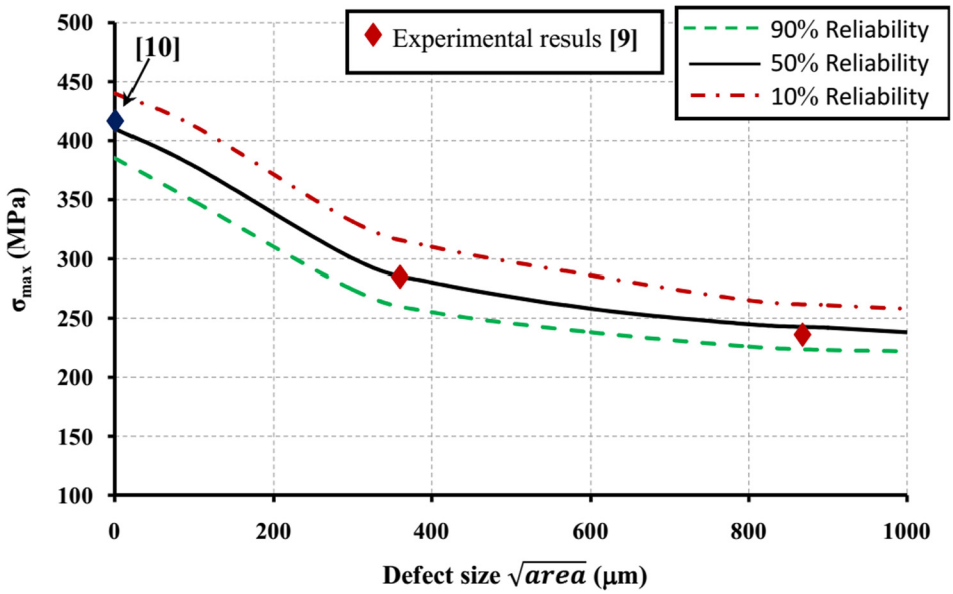

Fig. 12. Probabilistic Kitagawa–Takahashi diagram under tension loading ($R_\sigma = 0.1$) for the steel.

6.2.3. Torsion loading ($R_\sigma = -1$)

Under torsion load, the Crossland stress change is interpolated by:

$$\sigma_{eq}^{Cr}(r) = \frac{\tau_{D-1}}{\sigma_{D-1}} \times \tau_a \times \left(\frac{1}{(r/R)^4} + 1 \right) \tag{17}$$

At a depth a_w, the equation below becomes:

$$\sigma_{eq}^{Cr}(a_w) = \frac{\tau_{D-1}}{\sigma_{D-1}} \times \tau_a \times \left(\frac{1}{((R + a_w)/R)^2} + 1 \right) \tag{18}$$

Steel results are exposed in Fig. 14.

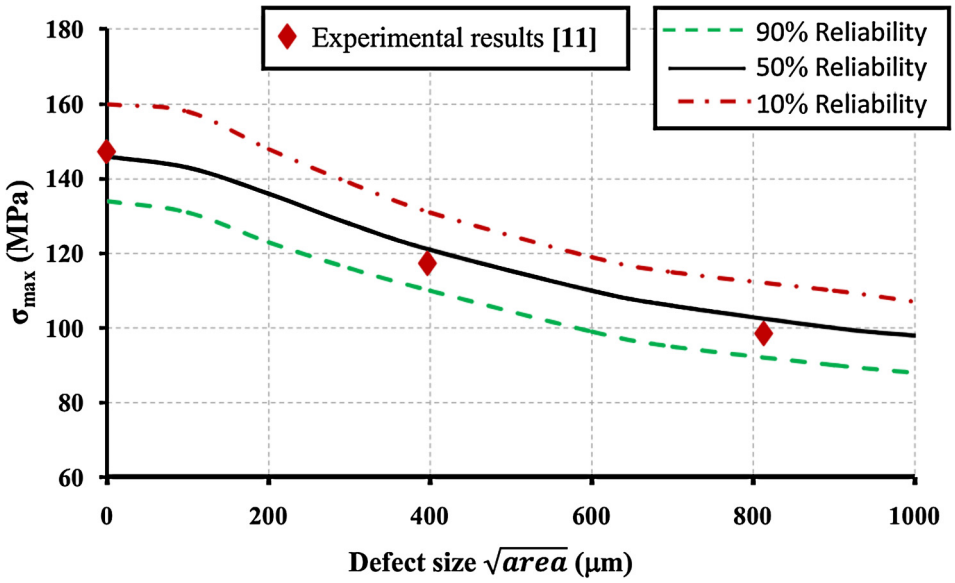

Fig. 13. Probabilistic Kitagawa–Takahashi diagram under tension loading ($R_\sigma = 0.1$) for the AS7G06-T6 aluminum alloy.

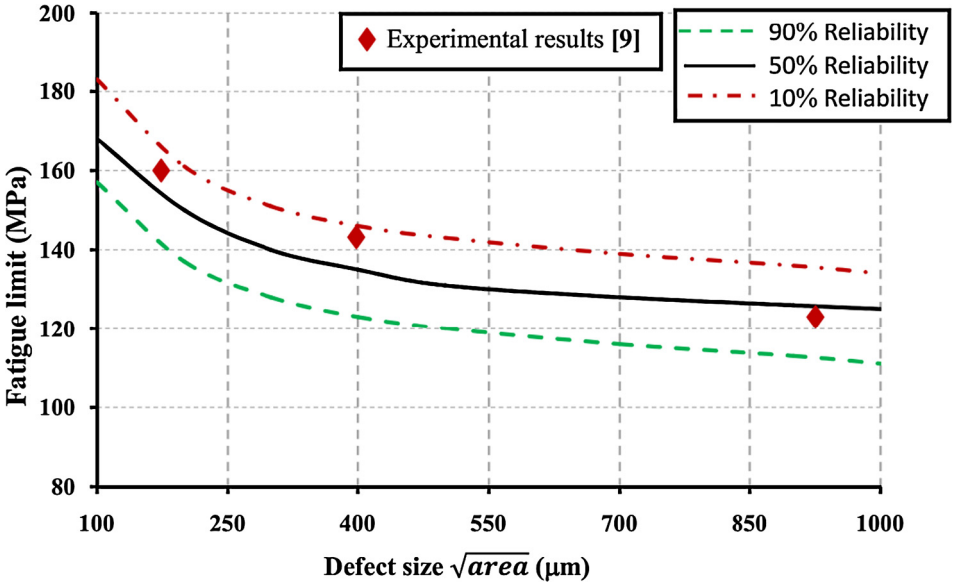

Fig. 14. Probabilistic Kitagawa–Takahashi diagram under torsion load for the steel.

For both tested materials, experimental points are in the spindle bounded by the 10 and 90% reliability curves. Consequently, the computed results are in accordance with experimental data. Moreover, the presented approach considers well the mechanical–geometrical parameters scatter. It is noted that, for a definite defect size, in the ranges 100 and 1000 µm, the scattering is carried by the load amplitude for both materials. Additionally, the scattering of the aluminum alloy is more significant. This agrees well with fatigue tests for the aluminum alloy with and without defect [11].

7. Sensitivity effects

The aim of this section is to extract relationships and interactions between the response (HCF strength of defect material) and diverse input parameters (a_w, σ_{D-1}, σ_a, and $\sqrt{area}$). In fact, the method allows investigating both the individual effects of each parameter and describing the interactions between them. To do it, we define the minimum and the maximum borders of every parameter. These borders are supposed variables and follow a normal distribution. A $C_v = 5\%$ is imposed for every input parameter (Fig. 15). Sixteen calculations of the HCF strength are needed for every load type. (Four input parameters with two levels ($2^4 = 16$).) The MINITAB software is exploited to examine the computed results. Fig. 16

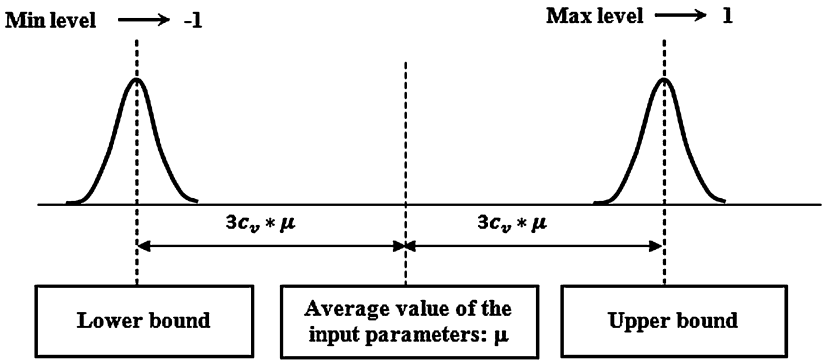

Fig. 15. Borders of input parameters.

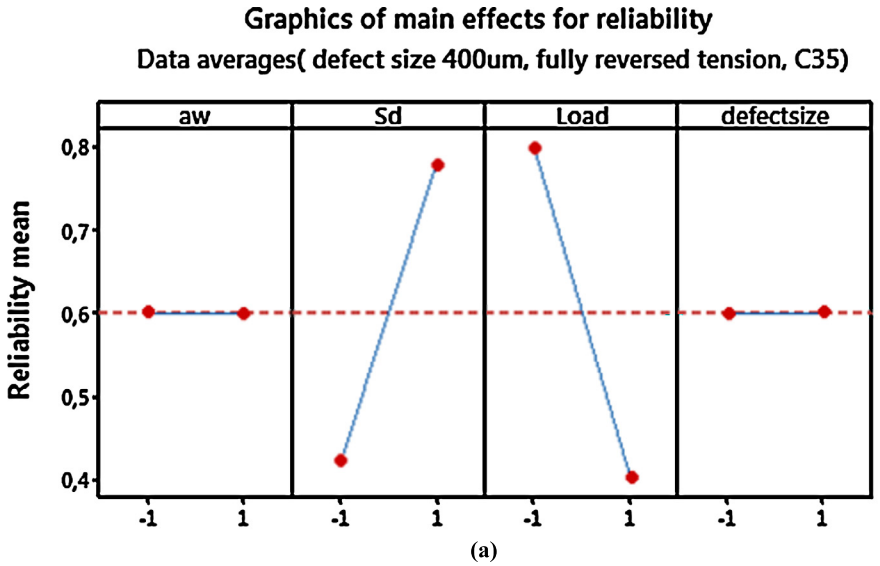

(a)

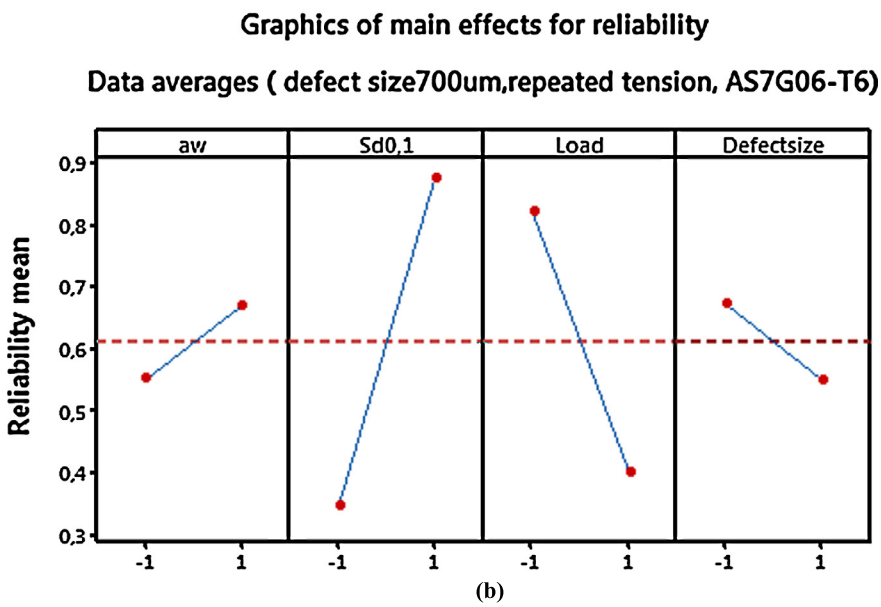

(b)

Fig. 16. Main effects plot on HCF strength: (a) C35 material under tension load, $\sqrt{area} = 400$ μm, $\sigma_a = 150$ MPa, (b) aluminum alloy under repeated tension, $R_\sigma = 0.1$, $\sqrt{area} = 700$ μm, $\sigma_{max} = 100$ MPa, AS7G06-T6, (c) C35 material under torsion load, $\tau_a = 145$ MPa, $\sqrt{area} = 400$ μm.

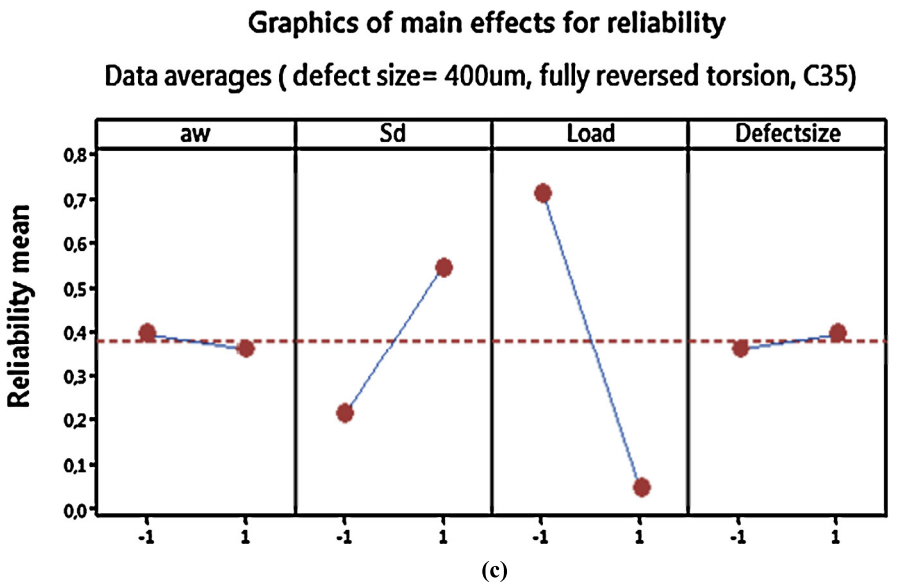

Fig. 16. (*continued*)

illustrates the main effects of the defect size, load amplitude, critical affected depth, and tension fatigue limit ($\sqrt{area}$, σ_a, a_w, and σ_{D-1}) on the HCF strength for the three simulated loadings.

For the defective C35 steel submitted to tension load ($R_\sigma = -1$, $\sqrt{area} = 400$ µm, $\sigma_a = 150$ MPa) (Fig. 16a), the scattering of both parameters σ_a and σ_{D-1} have a significant power on the HCF strength. However, the size and the a_w parameter scatter have no important effect on the HCF strength. As concerns the AS7G03-T6 aluminum alloy submitted to repeated tension ($R_\sigma = 0.1$, $\sqrt{area} = 700$ µm, $\sigma_{max} = 100$ MPa) (Fig. 16b), the scattering of the σ_{max} parameter has the major influence on the HCF strength. Moreover, the scattering of both the critical depth a_w and the tension fatigue limit σ_{D-1} have less influence than the scattering of σ_{max} on the HCF strength. However, the scattering of the sizes of defects has no significant consequence on the HCF strength.

For the steel submitted to torsion ($\tau_a = 145$ MPa, $\sqrt{area} = 400$ µm) (Fig. 16c), the scattering of both parameters τ_a and σ_{D-1} has an important consequence on the HCF strength. However, the scattering of the size and of the a_w parameter has no significant consequence on the HCF strength. Consequently, the fluctuation or the disturbance of the τ_a or and σ_{D-1} (one or and both parameters) has an important consequence on the HCF strength. However, the fluctuation or the disturbance of the defect size or/and the a_w (one or and both parameters) has no influence on the HCF strength.

Fig. 17 shows mutual interactions between input parameters (which are defect size, load amplitude, critical affected depth and tension fatigue limit ($\sqrt{area}$, σ_a, a_w, and σ_{D-1})) on the HCF strength for the three simulated loadings. Regarding the steel submitted to tension load (Fig. 17a), there is a big interaction between the $\sqrt{area}$ and the a_w parameters. Although the scattering effect of the $\sqrt{area}$ parameter is unimportant, its interaction with the critical affected depth remains significant.

For the AS7G03-T6 aluminum alloy submitted to repeated tension (Fig. 17b), we observe that there is a mutual interaction between the critical affected depth, the repeated tension fatigue limit, and the load amplitude (a_w, $\sigma_{D0.1}$ and $\sigma_{0.1\,max}$) on the HCF strength.

For the steel submitted to torsion loading (Fig. 17c), we observe that there are big mutual interactions between all the input parameters on the HCF strength.

We must point out that the conclusions made, in this section, are for a definite defect size and a given load amplitude. Such conclusions cannot be generalized to all defect sizes and all load amplitude.

8. Conclusions

In this paper, an innovative methodology has been proposed to compute the HCF strength of materials with defects. FE calculations were carried out to determine stress distributions around defects that are represented by surface semi spherical void. The changes of Crossland stress, from the defect to the specimen bulk, were interpolated by mathematical expressions depending on defect free fatigue limits, defect radius, and profundity from the defect. Those mathematical expressions were used to calculate defective fatigue limits based on the influenced length (affected depth). The HCF strength of material was calculated by the "strength load" approach via Monte Carlo sampling.

Probabilistic Kitagawa–Takahashi diagrams of materials with defects were determined by considering the scattering of the critical affected depth, the tension fatigue limit, the load amplitude, and the defect size, which are assumed to be normally distributed. The comparison between computed HCF reliabilities and experimental results shows an excellent conformity for

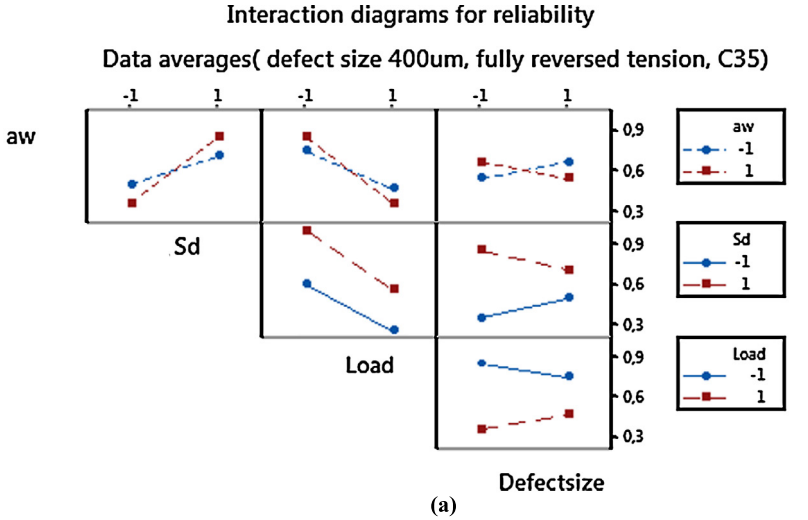

(a)

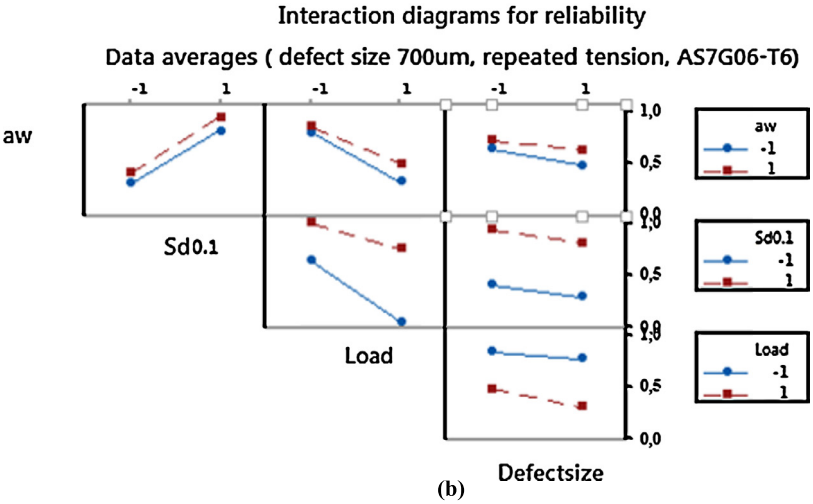

(b)

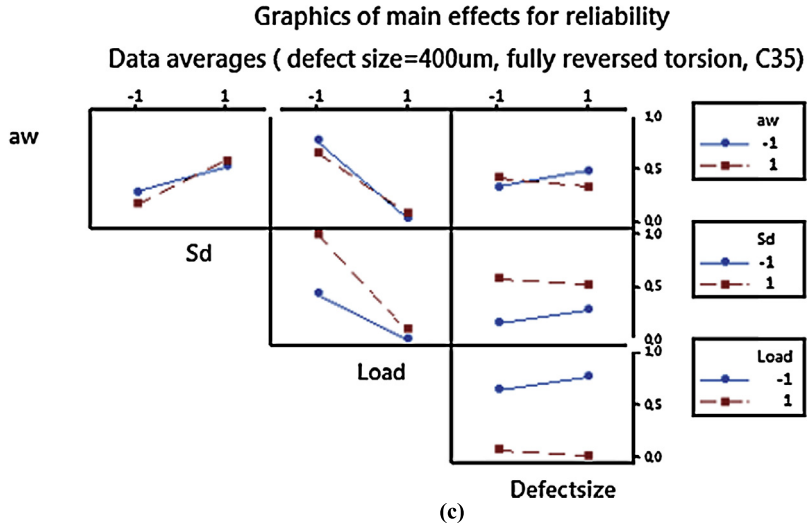

(c)

Fig. 17. Interactions between input parameters: (a) C35 material under tension load, $\sqrt{area} = 400$ µm, $\sigma_a = 150$ MPa, (b) aluminum alloy under repeated tension, $R_\sigma = 0.1$, $\sqrt{area} = 700$ µm, $\sigma_{max} = 100$ MPa, AS7G06-T6, (c) C35 material under torsion load, $\tau_a = 145$ MPa, $\sqrt{area} = 400$ µm.

both tested materials. Also, the sensitivity effects of defect size, affected depth, load amplitude, and tension fatigue limit, for predicting the fatigue strength of the material with defects, was presented.

The critical depth approach can be employed to compute the HCF strength of the defect material by computing the Crossland local stress at a depth a_w. Such an approach is preserved for multiaxial loadings and for diverse load ratios. Integration of the input parameters scattering effect allows the engineer to be engaged in a practical problem to assess the HCF strength in a safe and efficient process.

References

[1] H. Yaacub Agha, A.-S. Béranger, R. Billardon, F. Hild, High cycle fatigue behaviour of spheroidal graphite cast iron, Fatigue Fract. Eng. Mater. Struct. 21 (1998) 287–296.
[2] I. Chantier, R. Bobet, R. Billardon, F. Hild, A probabilistic approach to predict the very high cycle fatigue behaviour of spheroidal graphite cast iron structures, Fatigue Fract. Eng. Mater. Struct. 23 (1999) 173–180.
[3] A. Nasr, Ch. Bouraoui, R. Fathallah, Y. Nadot, Probabilistic high cycle fatigue behaviour of nodular cast iron containing casting defects, Fatigue Fract. Eng. Mater. Struct. 32 (2009) 292–309.
[4] W.K. Liu, Y. Chen, T. Belytschko, Y.J. Lua, Three reliability methods for fatigue crack growth, Eng. Fract. Mech. 53 (1996) 733–752.
[5] K.P. Oh, A diffusion model for fatigue crack growth, Proc. R. Soc. Lond. Ser. A, Math. Phys. Sci. 367 (1979) 47–58.
[6] E.D. Leonel, A. Chateauneuf, W.S. Venturini, P. Bressolette, Coupled reliability and boundary element model for probabilistic fatigue life assessment in mixed mode crack propagation, Int. J. Fatigue 32 (2010) 1823–1834.
[7] M. Liao, X.F. Xu, Q.X. Yang, Cumulative fatigue damage dynamic interference statistical model, Int. J. Fatigue 17 (1995) 559–566.
[8] Y.B. Xiang, Y.M. Liu, Application of inverse first-order reliability method for probabilistic fatigue life prediction, Probab. Eng. Mech. 26 (2011) 148–156.
[9] T. Billaudeau, Y. Nadot, G. Bezine, Multiaxial fatigue limit for defective materials: mechanisms and experiments, Acta Mater. 52 (2004) 3911–3920.
[10] A. Nasr, Y. Nadot, Ch. Bouraoui, R. Fathallah, M. Jouiad, Fatigue initiation in C35 steel: influence of loading and defect, Int. J. Fatigue 32 (2010) 780–787.
[11] P. Mu, Y. Nadot, C. Nadot–Martin, A. Chabod, I. Serrano-Munoz, C. Verdu, Influence of casting defects on the behaviour of cast aluminium AS7G06-T6, Int. J. Fatigue 63 (2014) 97–109.
[12] Y. Murakami, Metal Fatigue: Effects of Small Defects and Nonmetallic Inclusion, Elsevier Science Ltd, Oxford, UK, 2002.
[13] B. Crossland, Effect of large hydrostatic pressure on the tensional fatigue strength of fan alloy steel, in: Proceedings of International Conference on Fatigue of Metals, Institution of Mechanical Engineers, London, UK, 1956, pp. 138–149.
[14] Y. Nadot, T. Billaudeau, Multiaxial fatigue limit criterion for defective materials, Eng. Fract. Mech. 73 (2006) 112–133.
[15] A. Nasr, W. Hassine, Ch. Bouraoui, Fatigue limit assessment for defective materials based on affected depth, Metall. Res. Technol. 114 (2017) 505.
[16] M. Lemaire, A. Chateauneuf, J. Mitteau, Fiabilité des structures: couplage mécano-fiabiliste statique, Hermès, Paris, 2005.
[17] Y. Zhao, T. Ono, Moment methods for structural reliability, Struct. Saf. 23 (2001) 47–75.
[18] P. Bjerager, On computation methods for structural reliability analysis, Struct. Saf. 9 (1990) 79–96.
[19] H.P. Lieurade, La pratique des essais de fatigue, Pyc Livres, Paris, ISBN 2-85330-053-6, 1982 [in French].
[20] J. Schijve, Statistical distribution functions and fatigue of structures, Int. J. Fatigue 27 (2005) 1031–1039.
[21] C. Bathias, J.-P. Bailon, La fatigue des matériaux et des structures, Hermès, Paris, 1997 [in French].
[22] R. Ben Sghaier, Ch. Bouraoui, R. Fathallah, T. Hassine, A. Dogui, Probabilistic high cycle fatigue behaviour prediction based on global approach criteria, Int. J. Fatigue 29 (2007) 209–221.